Dynamics of highly charged ions interacting with surfaces

Bodewits, Erwin

Chapter 2

Electron dynamics relevant to HCI-surface interactions

The interaction of ions with surfaces is a very complex, dynamical many-body problem, which is especially true for highly charged ions (HCI) interacting with a surface. For that reason, a rigorous theoretical description of the ion surface interaction is beyond the scope of this thesis. In this chapter an overview of different processes of ion-surface interactions relevant to the understanding of the experiments presented in this thesis is given.

In section 2.1 the charge transfer processes are described, whereas 2.2 describes the classical over the barrier model.
In order to investigate the neutralization of HCI's metallic nano-capillaries were introduced. Here the idea was that an ion does not have enough time to become fully neutralized and deexcitated, allowing investigations to be done [30, 31]. Soon afterwards however, the amazing fact was found that ions could be guided through insulating capillaries without losing energy or charge. Section 2.4 deals with these nano-capillaries. All the units in this chapter are atomic units (a.u.) unless specified otherwise.

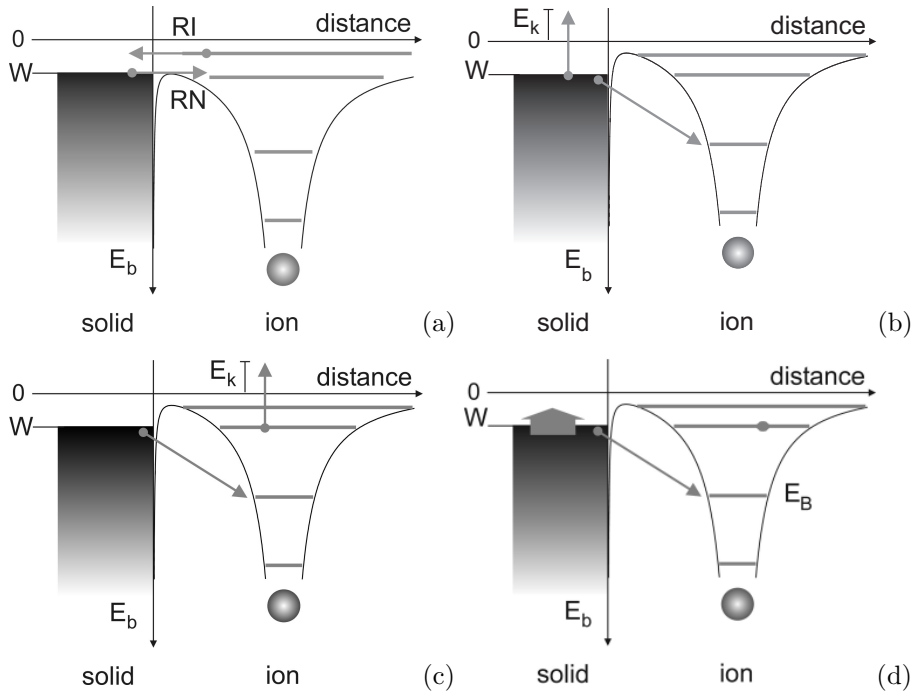

Figure 2.1: Electronic transitions between a surface and an ion. a: resonant neutralization (RN) and resonant ionization (RI). b: Auger neutralization (AN). c: Auger deexcitation (AD). d: collective excitations. For more details see text.

2.1 Charge transfer processes

Resonant transitions

When an ion approaches a surface, the potential barrier between the ion and surface decreases. At a certain point (defined in section 2.2) electrons can be resonantly transferred from and to the target. In the first case, when an electron is transferred from the surface to the ion, the process is called resonant neutralization (RN). In the second case, where an electron is removed from the ion thereby ionizing it even more, the process is called resonant ionization (RI). Both processes are shown in fig. 2.1(a). In this process no electrons are emitted. The rate Γ_R of the resonant electron transfer process from a solid perturbed by

the presence of an ion of charge q at a distance z in front of the surface is given, in the first order, by Fermi's golden rule (see e.g. [20]):

$$\Gamma_R = 2\pi |H_{f,i}|^2 \rho_f, \tag{2.1}$$

where ρ_f is the density of states of the metal resonant with the energy of the final atomic level, and $H_{f,i}$ gives the coupling between the metallic state ψ_i and the atomic state ψ_f:

$$H_{f,i} = \left\langle \psi_f \left| -\frac{q}{r} \right| \psi_i \right\rangle, \tag{2.2}$$

where the operator is the Coulomb potential of the ion nucleus acting on an electron at distance r. Since the initial and final wavefunctions are located at different centers and drop exponentially with increasing distance from the surface, so does the matrix element $H_{f,i}$. Therefore, for sufficiently large z, the resonant transfer rate Γ_R will also drop exponentially:

$$\Gamma_R(z) = \Gamma_R(0) e^{-\alpha_R z}, \tag{2.3}$$

where $\Gamma_R(0)$ denotes the maximum rate, at $z = 0$, and α_R is the decay length of the matrix element $H_{f,i}$. Typical $\Gamma_R(0)$ rates range from 0.01 to 0.1 a.u. ($10^{14} - 10^{15}$ s^{-1}).

Auger neutralization

When an electron is captured by the projectile into a more strongly bound state, and another electron from the target is ejected into the vacuum using the available energy. This process, called Auger neutralization (AN), is schematically shown in fig. 2.1(b). The maximum kinetic energy E_k of the emitted electron occurs when both electrons originate from the Fermi level of the target and is given by $E_k = E_b - 2W$. Here E_b is the binding energy of the electron in the projectile and W the work function of the target. Just like for resonant transitions, the Auger neutralization rates depend on the coupling between the final projectile state $|\psi_f\rangle$ and the initial state at the target $\langle\psi_i|$. The coupling matrix H_{fi} however, is now determined by the repulsive electron-electron interaction. For large z, the Auger neutralization rates decay exponentially, just like in the case of resonant transitions

$$\Gamma_{AN}(z) = \Gamma_{AN}(0) e^{-\alpha_{AN} z}. \tag{2.4}$$

For small z the structure of the wave functions has to be taken into account. Typical Auger neutralization rates $\Gamma_{AN}(0)$ are in the range between 0.01 and 0.5 a.u. [32].

Auger de-excitation

Similar to Auger neutralization, an electron from the target is captured into a stronger bound state of the projectile. However, instead of ejecting an electron out of the target, a less bound electron is emitted from the projectile. The maximum energy is $E_k = E_b - W - E_b^{'}$, where E_b and $E_b^{'}$ are the binding energies of the electrons in the stronger and weaker bound state, respectively. Since this process is quite similar to Auger neutralization, the rates for Auger de-excitation are comparable to the Auger neutralization and range between 0.01 and 0.5 a.u. The Auger de-excitation process is shown in fig. 2.1(c).

Collective excitations

Collective excitations are processes in which a conduction band electron is transferred into a lower lying level in the incoming ion, while the energy difference is used to excite a plasmon (Fig. 2.1(d)). The energy of the plasmon is provided by the potential energy released by the neutralization of the ion $E_p = E_I - W - \epsilon$, where ϵ is the energy of the conduction band electron, and E_I is the ionization energy of the final atomic state. As no electrons are emitted during this process, the creation of a plasmon shows up as a dip in the energy distribution of secondary electrons emitted during ion bombardment of the surface. The collective excitations play only a minor role however compared to the other processes [33].

Autoionization

In order for autoionization to take place, two electrons are required in an excited state of the projectile (see fig. 2.2(a)). When one of the electrons falls to a stronger bound state in the projectile, the excess energy is used to eject the other electron into the vacuum. The energy of this electron is given by $E_k = E_b - E_b^{'}$, which is the difference in binding energies between the initial and final state. Just like the decay rate for resonant transitions (eq. 2.1), the autoionization decay rate is given by Fermi's golden rule. In this particular case however, the density of final states is purely atomic and therefore well defined. This results in electrons being emitted with well defined discrete energies [34, 35]. Furthermore, since autoionization is an intra-atomic process, the distance to the surface does not play a role in the decay rate until the ion approaches the surface very closely. Depending on the states involved, typical rates range between 0.001 and 0.01 a.u.

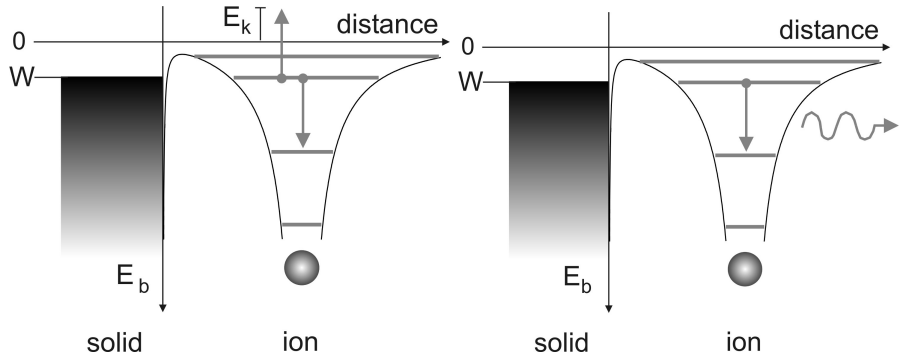

Figure 2.2: Transitions which involve the ion only. A: Autoionization. B: Radiative decay. For more details see text.

Radiative decay

Another way of how an ion can de-excite is by means of radiative decay. In this process a photon is emitted, carrying away the excess energy when an electron is transferred to a stronger bound state. This process is depicted in fig. 2.2(b). The wavelength of this emitted photon is given by $\lambda = hc/(E_B - E_B^{'})$, where E_B and $E_B^{'}$ are the initial and final state binding energies. The rate of radiative decay is dependent on the nuclear charge Z and increases for hydrogen-like wave functions as Z^4. Therefore, this process becomes more important for the heavier and more highly charged ions. Typical rates for hydrogen like ions are $\Gamma_P \simeq 4 \cdot 10^{-7} Z^4/n^{4.5}$.

2.2 Classical over-the-barrier model

The classical over-the-barrier (COB) model was originally developed to describe the charge transfer between atoms and multiple charged ions [36]. Later on, this model was extended to describe the interaction of multiply charged ions in front of surfaces [37]. This section describes the main ingredients of this model.

According to the classical over-the-barrier model, electrons are resonantly captured from a surface into the atomic levels of an incoming ion, as soon as the potential barrier is reduced below the work function W of the surface. The reduction of the ion charge by the electron capture is increasing the height of the potential barrier on its turn, making it necessary for the ion to approach the surface closer again in order to repeat the process of electron capture. This way, multiply charged ions lose their charge in a stepwise manner by consecutive capture of conduction or valence electrons. At the same time, electrons can be resonantly lost to unoccupied states of the surface as well, which is also taken into account by the COB model. Also the subsequent ion relaxation of the excited ion is taken into account. Putting all this together, the neutralization distance in front of a surface and the atomic levels in which the electrons are captured can be evaluated as briefly summarized in the following.

The potential barrier between the surface and the ion as seen by an electron -e, is created by the potential of the ion with charge state +q and the potential of the image charges of the ion -q and the active electron +e, as shown in fig. 2.3. The image charges are formed when an ion is in front of the surface and attracts free electrons in the target towards the surface. This creates an electron cloud which screens the surface from the incoming ion. In the adiabatic limit, when the velocity of the ion v_i is much smaller than the Fermi velocity v_f of

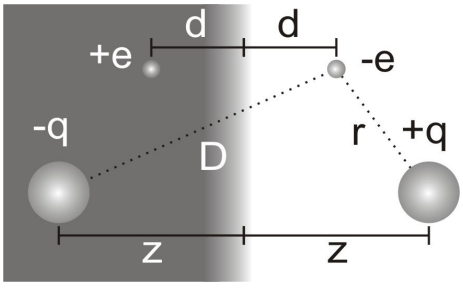

Figure 2.3: Classical screening of a charge in front of a conductor

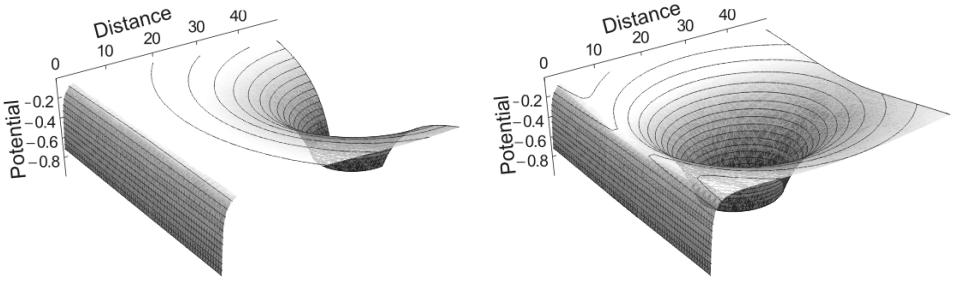

Figure 2.4: The potential V_T for a ion with $q = 10$ at a distance of 50 a.u. (left figure) and 24 a.u. (right figure) of the surface.

the target electrons, the screening effect of the electron cloud can classically be described by an electrostatic potential V_i. In order to use this concept, an image plane needs to be defined. Because there is no hard limit of where the surface starts or ends, the jellium edge is taken for this purpose and is defined as the point where the target electron density is dropped to half its original value [38]. Typically this distance is approximately half an atomic layer above the topmost atomic layer.

The total potential V_T experienced by an electron at a distance r in front of a surface, is then formed by the sum of the ion potential at distance +z from the surface, the ion image potential positioned at -z and at a distance D of the electron and the self image potential of the electron at a distance of $2d$ (see fig. 2.3). In order to simplify this picture, the electron is assumed to be positioned between the ion and surface. Using the substitutions $r = z - d$ and $D = z + d$, one finds the one dimensional potential

$$V_T = -\frac{q}{z-d} + \frac{q}{z+d} - \frac{1}{4d}. \tag{2.5}$$

Figure 2.4 and 2.5 show the total potential V_T for a ten–fold charged ion when it is located at $z = 24$ a.u. and at $z = 50$ a.u. in front of the surface. The typical work function for a metal, which is around 5 eV, is also shown for illustrative purposes.

The distance at which resonant electron capture starts, the so called critical distance z_0 can be estimated as follows: first the position of the saddle point is determined, by setting the derivative of the total potential to zero, i.e. $\partial V_T /$

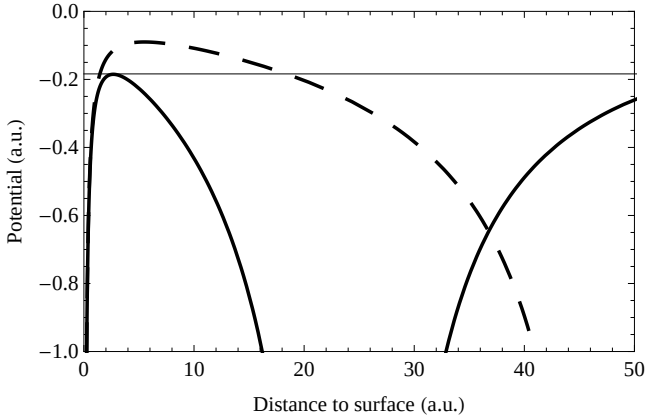

Figure 2.5: Intersection of figure 2.4 along the ion-surface normal. Also shown is the typical work function for a metal. As can been seen, at a distance of 24 a.u. electrons can go over the barrier for an ion with $q = 10$.

$\partial d = 0$. To a very good approximation, the position of the saddle point is then given by [37]

$$d_s = \frac{z}{\sqrt{8q+2}} \approx \frac{z}{\sqrt{8q}}. \tag{2.6}$$

Inserting this distance back into equation 2.5, one finds the potential at the saddle point position to be

$$V_s = -\frac{\sqrt{8q+2}(16q+1)}{4z(8q+1)} \approx -\frac{\sqrt{2q}}{z}. \tag{2.7}$$

Setting this potential equal to the work function W of the surface, gives the distance z_c at which renonant electron capture takes place according to the COB model

$$z_c = \frac{\sqrt{8q+2}}{2W} \approx \frac{\sqrt{2q}}{W}. \tag{2.8}$$

The principal quantum number n of the state into which first neutralization takes place can be calculated in a hydrogenic approximation and is found to be [1]

$$n = \frac{q}{\sqrt{2W}} \left(1 + \frac{q - \frac{1}{2}}{\sqrt{8q}}\right)^{-\frac{1}{2}} \approx \frac{q}{2\sqrt{W}}. \tag{2.9}$$

The image charge interaction introduced above does not only influence the total potential experienced by an electron (eq. 2.5), but also interacts with the ion. Due to this image charge, the ion accelerates towards the surface. The force exerted on an ion with charge q and at distance z from the surface equals $q^2/(4z^2)$. Assuming single electron capture (stepwise capture) and full shielding of one unit of charge of the incoming ion, the total image energy E_{im} gained by the ion is [1]

$$E_{im} = \int_{\infty}^{z_n} -\frac{q^2}{4z^2}\, dz \approx \frac{q^{3/2}}{3}\frac{W}{\sqrt{2}}. \tag{2.10}$$

The velocity gained puts a lower limit on the energy at which an ion approaches a surface and thus setting a maximum on the time the ion can spend in front of the surface before impact. For very slow, highly charged ions, this can also have a dramatic effect on the impact angle on a surface as well. For U^{92+} ions approaching a metal surface, which is a system foreseen to be studied in the future at *GSI*, the "image" energy is 1 keV.

2.2.1 Insulating surfaces

When going from a metallic to an insulator surface, the dielectric response has to be considered [39]. Incorporating this into the classical over the barrier model modifies the total potential (eq. 2.5) as follows:

$$V_T = -\frac{q}{z-d} + \left(\frac{q}{z+d} - \frac{1}{4d}\right)\frac{\epsilon-1}{\epsilon+1}. \tag{2.11}$$

The change in total potential also changes the distance at which an electron is captured. The modified electron capture distance for an insulator is given by

$$z_c = \frac{1}{2(\epsilon+1)I}\sqrt{8q\epsilon(7+\epsilon)}, \tag{2.12}$$

where I is the ionization potential. Fig. 2.6 shows what kind of effect these modifications (reduced dielectric response and higher electronic binding energies of the target) have by comparing LiF ($\epsilon \sim 9, I = 11.8$ eV) to a typical metal ($W \sim 5$ eV)

2.3 Level shifts

The image charge interaction introduced in the previous section does not only attract an ion towards the surface, but also causes a shift in the binding energies

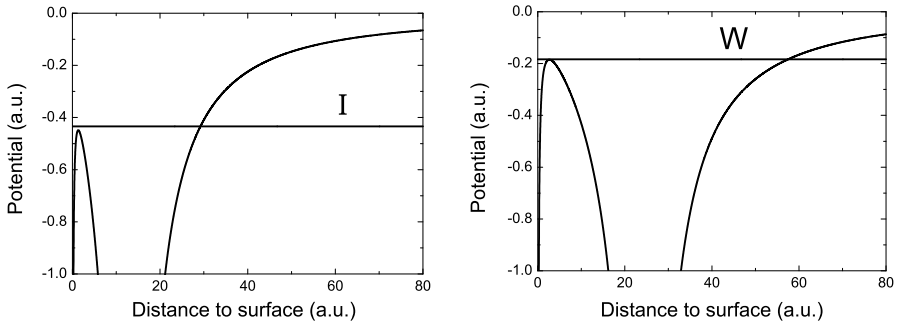

Figure 2.6: Left: the potential experienced by an electron in front of an insulating surface with ϵ=9, I =12 eV. The location of the ion ($q = 10$) in front of the surface is where the first capture takes place according to eq. 2.12. Right: Same, but for a metal with $W = 5$ eV and a critical distance according to eq. 2.8.

in the ion. This is caused by the fact that the electron involved feels its own attractive image charge as well as the repulsive image charge of the ion. When the distance R between the ion and surface is still over a few a.u., the shift in binding energy is in first order given by [3]

$$\Delta E = \frac{2Z - 1}{4R}, \tag{2.13}$$

where Z is the effective charge seen by the electron. Fig. 2.7 shows an example for a doubly excited helium atom, where Z_{eff} is taken to be 1.65 [35]. This change in binding energy can thus cause a shift in the level towards the fermi level of the surface, thereby prohibiting resonant neutralization and/or promoting resonant ionization.

In the moving frame of the ion, the target density of electronic states differs with respect to the density of states in the laboratory reference frame. In general, this effect is described from a momentum point of view, using a Galilean transformation [3, 35, 40]. In the laboratory reference frame, the electrons of the target are occupying the Fermi sphere, whose center lies at the origin. In the moving frame of the ion however, this center is shifted in the opposite direction of the ion velocity. Due to this Galilean shift, the energy of the electrons is transformed according to

$$E(\vec{v}) = \frac{1}{2}v^2 = E_F - \vec{v}_F \cdot \vec{v}_i + \frac{1}{2}v_i^2, \tag{2.14}$$

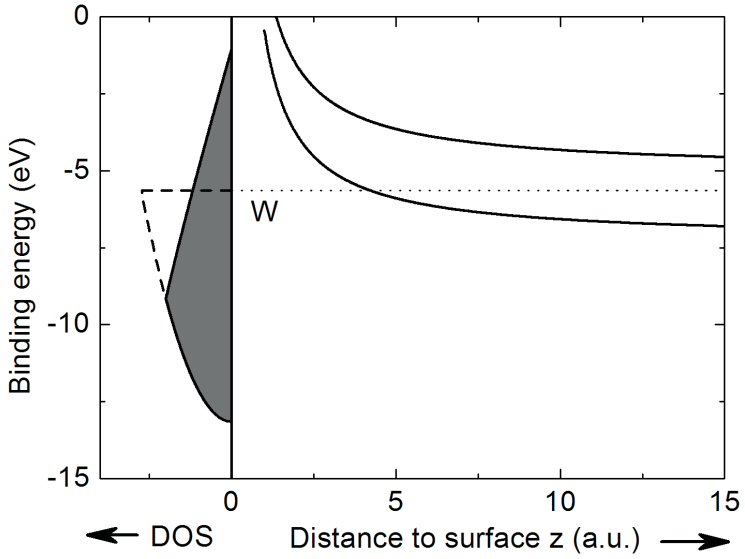

Figure 2.7: On the left side the shifted DOS of a metal due to the velocity of the ion is shown, as well as the unperturbed DOS (dotted). The right side shows the shift in binding energy due to the image charge interaction.

where v_F is the Fermi velocity and v_i the ion velocity For grazing incidence scattering the Fermi sphere shift due to $v_{i\perp}$ can be neglected, and $v_i \approx v_{i\parallel}$. As a result of the shift due to the velocity of the ion, the energy of the Fermi electrons varies in the range between [41]

$$\frac{1}{2}(v_F - v_i)^2 \leq E_F \leq \frac{1}{2}(v_F + v_i)^2. \tag{2.15}$$

It can be shown that the occupation probability $g(E, v_i)$ of metal states with energy E for an ion velocity v_i, in the moving ion reference frame, is given by [40]

$$\begin{aligned} g(E, v_i) &= 1 && 0 \leq \varepsilon \leq (1-\nu)^2. \\ &= \frac{1}{2} + \frac{1-\nu^2}{4\nu\sqrt{\varepsilon}} - \frac{\sqrt{\varepsilon}}{4\nu} && (1-\nu)^2 \leq \varepsilon \leq (1+\nu)^2. \\ &= 0 && \varepsilon \geq (1+\nu)^2. \end{aligned} \tag{2.16}$$

where $\nu = v_i/v_F$ and $\varepsilon = E/E_F$ are the relative velocity and energy. In figure 2.7 a modified density of states is shown for a moving ion in front of a typical metal surface. Due to the modified DOS, a moving ion sees a lower work function, which allows electrons to be resonantly captured from the surface at a larger distance compared to a non moving ion. This on its turn gives the ion more time to capture electrons, thereby emitting more electrons as well.

2.4 Capillaries

In order to understand the guiding of ions through capillaries, fig. 2.8 is often used as a sketch of the generic scenario. Two different regions are considered, referred to as the scattering and guiding region. The guiding region is sometimes referred to as the exit region as well. In the scattering region the ions interact with the walls of the capillary, creating a so called entrance patch. It is assumed that most of the deposited charge is located at or near this entrance patch. The deposited charge creates an electric field, thereby deflecting the ions. Inside the capillary however, the electric field is assumed to play a minor role due to the fact that an infinite tube with homogenous charge distribution is field free. At the exit of the capillary however, this symmetry is broken, which introduces a defocusing electric field. Although fig. 2.8 sketches a relative simple picture, the actual modeling of the guiding through capillaries is not. The main difficulty

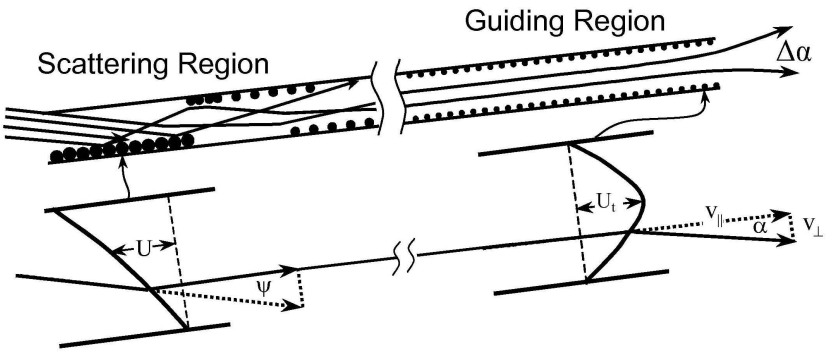

Figure 2.8: The ions enter the capillary from the left, depositing charge on the wall. After a few ions hit the wall the entrance patch is strong enough to deflect the further incoming ions.

lies here in the fact that simulations would need to cover a process where the fastest process is 18 orders of magnitude faster than the slowest: the microscopic charge up and hopping of charge takes place on a time scale of (sub)fs, whereas the characteristic (bulk) discharge time of the capillaries can take up to $\geq 10^3$s. In between these time ranges, the ion passes through the capillary ($10^{-10}s$) and other ions enter/interact with the same capillary (10^{-1}s). Since it is impossible to simulate this at present, instead simulations are done which try to interrelate the microscopic description of ion-surface impact with macroscopic properties of charge-up and transport [42, 43].

Although a detailed description of the charge-up and guiding of ions through nano capillaries is beyond the scope of this thesis, a short description of the deflection in the scattering region and the defocusing at the end of the guiding region is given below.

Scattering region

In order to find the fraction of transmitted ions through a capillary, we take into account the incident current J_{in} entering the capillary, the discharge current J_{dis} due to the bulk and surface conductivity and the propagated current J_p transmitted through the capillary. The incidence charge is allowing the charge patch $Q_{acc}(t)$ to grow (acc in the subscript for accumulated), but will eventually be limited by the discharge and transmitted current. The time evolution of this charge patch, assuming a constant beam current coming in, is given by [44]

$$\frac{dQ_{acc}(t)}{dt} = J_{in} - J_{dis}(t) - J_p(t). \tag{2.17}$$

At first J_{dis} was taken proportional to the accumulated charge Q_{acc}. However, this did not account for the fact that the transmitted fraction of ions decreased noticeably with increasing incidence angle. Therefore, an exponential dependence of the discharge current J_{dis} on the square root of the charge was adopted [45]:

$$J_{dis}(t) = \frac{Q_{acc}(t)}{\tau_{dis}} e^{\sqrt{\frac{Q_{acc}(t)}{Q_{dis}}}}. \tag{2.18}$$

Here, Q_{dis} is a charge constant and τ_{dis} the time constant characteristic for the capillary discharge.

From experiments done [44, 45], it turned out that current which propagated through the capillary J_p, depended exponentially on the perpendicular ion energy $E_\perp = E_p sin^2\psi$ with E_p the energy of the projectile and ψ the incidence angle. In this case, the ion is lost if its perpendicular energy $E_\perp$ is higher than

qU with q the charge of the incoming ion and U the potential in the scattering region. Using this fact, the potential inside the capillary was replaced by the deposited charge and a capacity, $C_e = Q_d/U$, which gives the fraction of transmitted ions

$$f(\psi) = f_0 e^{-\frac{C_e E_p}{q Q_d} sin^2\psi}. \tag{2.19}$$

Here f_0 is determined empirically and is the fraction of ions transmitted at $\psi = 0$. Defining $\psi_c \approx sin^2\psi_c = Uq/E_p$, where ψ_c is the so called characteristic guiding angle, the fraction of transmitted ions takes the simple form

$$f(\psi) = f_0 exp\left(-\frac{sin^2\psi}{sin^2\psi_c}\right) \tag{2.20}$$

At ψ_c the intensity drops to a value of 1/e with respect to the intensity at 0° incidence angle.

Exit region

From experiments it became obvious that the angular distribution of ions propagated through the capillaries is larger than expected from merely the aspect ratio of the capillaries [44, 46, 47]. In order to describe this, the angular distribution $dY/d\Omega_\alpha$ of the transmitted ions is introduced. Similar as in eq. 2.20, the exponential function

$$\frac{dY(\alpha)}{d\Omega_\alpha} = \frac{dY_{max}}{d\Omega} e^{-\frac{E_p}{q_f U_t} sin^2\alpha}. \tag{2.21}$$

describes the transmitted fraction. Here α is the emission angle relative to the capillary axis, and q_f the final charge state of the projectile emerging from the capillary. Making the same substitution as done for the transmitted fraction, this gives the Gaussian equation

$$\frac{dY(\alpha)}{d\Omega_\alpha} = \frac{dY_{max}}{d\Omega} e^{-\frac{sin^2\alpha}{sin^2\alpha_t}}. \tag{2.22}$$